ULTRASONIC IMAGING 14, 249-275 (1992)

OPTIMUM NONLINEAR SIGNAL DETECTION AND ESTIMATION IN THE PRESENCE OF ULTRASONIC SPECKLE

Constantine Kotropoulos and Ioannis Pitas

Department of Electrical Engineering
University of Thessaloniki
Thessaloniki 540 06, Greece

A unified approach to the design of nonlinear filters for speckle suppression in ultrasound B-mode images is presented. The detection of the (lesion) signal is formulated as a binary hypothesis-testing problem. The structure of the optimal decision rules is derived both in the case where the lesion signal is assumed either a constant or random variable. In the case of a constant signal, the maximum likelihood (ML) estimator and the optimal L-estimator are derived. In the case of a random lesion signal, the maximum a posteriori probability estimator of the lesion signal has also been found. Experimental results verify the superiority of the proposed ML-estimator and the L-estimator over the straightforward choice of an arithmetic mean for speckle filtering in simulated tissue mimicking phantom ultrasound B-mode images.

Key words: B-mode images; detection; estimation; L-estimator; maximum likelihood (ML) estimator; maximum a posteriori probability (MAP) estimator; optimal decision rules; Rayleigh statistics; receiver operating characteristic (ROC); ultrasonic speckle.

1 INTRODUCTION

Speckle noise is a special kind of noise encountered in images formed by laser beams, in radar images as well as in envelope-detected ultrasound B-mode images. It is an interference effect caused by the scattering of the ultrasound beam from microscopic tissue inhomogeneities [1,2]. There is a rich literature on ultrasound image filtering and analysis. Smith et al. have dealt with the derivation of the contrast/detail function both experimentally as well as theoretically. They have shown that the same signal-to-noise ratio is obtained either by treating the detection of a low-contrast disk-shaped lesion embedded in ultrasonic speckle in the context of statistical decision theory or by evaluating the first and second-order moments of speckle. Smith et al. have concluded that the contrast/detail results for the envelope detection in diagnostic ultrasound are almost identical with the results for square law detection with the later serving as upper limit for performance in lesion detection [3]. The tissue architecture has been described

0161-7346/92 $5.00

by the average spacing between semiperiodic tissue scatterers, the ratio of specular to diffuse backscatter intensities and the fractional standard deviation in the specular backscatter intensity under the assumption of generalized Rician statistics [4,5]. The concepts of the Receiver Operating Characteristic (ROC) curve, the ideal observer, the ideal observer signal to noise ratio constructed from the laboratory measurements and the application of the ideal observer approach to clinical diagnostic systems have been discussed by Wagner [6]. The implications of power functions of the echo envelope signal and the logarithm of the echo envelope signal on the first and second order statistics have been derived by Thijssen et al. [7]. It has been found both theoretically and practically, that the intensity display (i.e., a power law transform of 2) corresponds to the optimal transform for a low contrast lesion. The detection of focal lesions from the point of view of communication systems has been considered by the same author [8]. Pattern recognition techniques have been used by Raeth et al. [9] and Insana et al. [10] to determine the smallest number of tissue parameters for the detection and classification of the presence of disease. A number of adaptive filters, i.e., filters which adjust their smoothing properties at each point of the image according to the local image content, have been proposed for ultrasonic speckle suppression by Bamber and Daft [11], Loupas et al. [12], and Koo and Park [13]. The improvement of the performance of adaptive filters based on the local coefficient of variation of the observed image has been studied by Lopes et al. [14]. Homomorphic filtering or signal adaptive median (SAM) filtering could also be applied in speckle suppression [15].

As far as ultrasonic speckle is concerned, all the filters proposed so far are applied to the displayed image data and are based on empirically chosen estimators (e.g. sample mean [11,13] or weighted median [12]). On the contrary, the approach followed here focuses on the raw ultrasound signal just after envelope detection and derives optimum signal estimators based on the statistical properties of the data. This approach has two distinctive advantages:

1. Accurate modeling. By processing raw envelope-detected data, it is possible to use an accurate model of their statistics. This is not the case with the displayed image data that have undergone excessive manipulation (e.g., logarithmic compression, low and high-pass filtering, postprocessing, etc.) to such an extent that modeling of their statistics becomes very difficult.

2. Computational efficiency. In commercial scanners, the clock rate of the digitized envelope-detected signal is at least two times slower than the corresponding rate of the video signal [16]. Therefore, from a hardware point of view, it makes more sense to process the envelope-detected signal.

However, a serious cost is paid by processing raw-envelope detected data. It has been shown that the mean grey level and the lateral speckle size depend greatly on the distance to the transducer [17]. Although, in ultrasound B-mode images the above-mentioned diffraction effects can be neglected in a first order of approximation, when a clinical image is processed the characteristics of any filter have to be adapted in order to take into account the dependence on the distance to the transducer.

The main contribution of this paper is in the area of signal estimation, through the design of optimal nonlinear filters for speckle removal in ultrasound B-mode images and

the derivation of their properties. However, the important problem of signal detection is also examined. More specifically, the starting point is modeling of ultrasonic speckle as multiplicative noise [18]. At a first approach, the signal is assumed to be constant and the noise term to be Rayleigh random variable having unity expected value. The detection of the constant signal is expressed as a binary hypothesis-testing problem. The structure of the optimal decision rule is derived by comparing the likelihood ratio to a constant threshold. The optimal decision rule is examined whether it is a uniformly most powerful test or not. The receiver operating characteristics for the optimal decision rule are derived by evaluating theoretically the probability of false alarm and the probability of detection without invoking the central limit theorem by contrast to the approach of Smith et al. [3]. The problem of estimating the constant signal is also considered. It is proven that the maximum likelihood (ML) estimator of the signal is the L_2 mean filter [19] multiplied by a constant scaling factor. The expected value and the variance of this estimator have been evaluated. The mean-squared-error (MSE) in estimating the constant signal by using the ML-estimator has also been calculated. The use of an L-estimator of the constant signal is proposed. L-estimators are defined as linear combinations of the order statistics, i.e., the observations arranged in ascending order of their magnitude inside the filter window [20]. The L-estimator that minimizes the mean-squared-error between the L-estimator output and the signal is designed. The connection between the ML-estimator and the L-estimator is demonstrated. At a second approach, the (lesion) signal is assumed to be random variable. The structure of the optimal decision rule is again derived. The maximum a posteriori probability (MAP) estimator of the random signal has also been found.

The outline of this paper is as follows. Section 2 describes the detection of the constant signal. Section 3 describes the estimation of the constant signal. The case of a random true signal is considered in section 4. Experimental results are included in section 5. Conclusions are drawn in section 6.

2 DETECTION OF A CONSTANT SIGNAL FROM SPECKLE

Let z be the envelope-detected observed signal, m be the signal and n be a noise term statistically independent of m. It is assumed that the signal m is related to the observation z by:

$$z = mn \tag{1}$$

The probability density function (pdf) of the observed random variable (r.v.) z is considered to be Rayleigh:

$$f_z(z) = \frac{z}{\sigma^2}\exp[-\frac{z^2}{2\sigma^2}], \quad z > 0 \tag{2}$$

The expected value of the r.v. z and its variance are [21]:

$$\mathrm{E}[z] = \sigma\sqrt{\pi/2} \tag{3}$$

$$\mathrm{var}[z] = \sigma^2(\frac{4-\pi}{2}) \tag{4}$$

The following lemma can be easily proven:

Lemma 1 *If the signal m is constant and equals to $\sigma\sqrt{\pi/2}$ and the noise term n is Rayleigh r.v. having unity expected value and variance $\frac{4-\pi}{\pi}$, then the pdf of the r.v. z is given by (2).*

In the following, model (1) will be used.

2.1 Structure of the Optimal Detection Rule

Let us assume that we have a set of N observations $z_1, z_2, \ldots, z_N$ denoted by a vector $\mathbf{z} = (z_1, z_2, \ldots, z_N)^T$ in the observation space $\mathcal{R}^N$. Let $\mathbf{n} = (n_1, n_2, \ldots, n_N)^T$ be a vector of N independent identically distributed Rayleigh noise random variables. Let us assume the following two hypotheses:

$$\begin{aligned} H_0 : \mathbf{z} &= m_0 \mathbf{n} \\ H_1 : \mathbf{z} &= m_1 \mathbf{n} \end{aligned} \tag{5}$$

created by the probabilistic transition mechanisms:

$$f_{z_i|H_k}(Z_i|H_k) = \frac{Z_i}{\sigma_k^2} \exp[-\frac{Z_i^2}{2\sigma_k^2}] \quad Z_i > 0, \;\; i = 1, \ldots, N \;\; k = 0, 1 \tag{6}$$

Under the hypothesis H_0, the constant signal m_0 equals to $\sigma_0\sqrt{\pi/2}$ and under the alternative hypothesis H_1, we have $m_1 = \sigma_1\sqrt{\pi/2}$. It must be noted that the pixels constituting an ultrasound B-mode image are generally correlated. The correlation between image pixels can be exploited if second-order statistics, i.e., the autocorrelation or the autocovariance function are included in the problem formulation. This is the case with the lesion signal-to-noise ratio which has been studied thoroughly in [3]–[7]. In the context of statistical decision theory the exploitation of the correlation between pixels would be possible, if a functional description of the correlation existed. But unfortunately, such a model has not yet been proposed. Therefore, the following analysis is based on the independence assumption like the treatment of Smith et al. [3] and Thijssen [8].

The Bayes criterion [22] leads to the likelihood ratio test (LRT):

$$\Lambda(\mathbf{Z}) = \frac{f_{\mathbf{z}|H_1}(\mathbf{Z}|H_1)}{f_{\mathbf{z}|H_0}(\mathbf{Z}|H_0)} \underset{H_0}{\overset{H_1}{\gtrless}} \theta \tag{7}$$

or equivalently to the log-likelihood ratio test:

$$l(\mathbf{Z}) = \ln \Lambda(\mathbf{Z}) \underset{H_0}{\overset{H_1}{\gtrless}} \ln \theta \tag{8}$$

By substituting Eq. (6) into Eq. (8) the following optimal decision rule results:

$$\sum_{i=1}^{N} Z_i^2 \underset{H_0}{\overset{H_1}{\gtrless}} \frac{2\sigma_0^2\sigma_1^2}{\sigma_1^2-\sigma_0^2}(\ln\theta - 2Nln\frac{\sigma_0}{\sigma_1}) = \gamma \quad \text{for } \sigma_1^2 > \sigma_0^2 \tag{9}$$

$$\sum_{i=1}^{N} Z_i^2 \underset{H_0}{\overset{H_1}{\lessgtr}} \frac{2\sigma_0^2\sigma_1^2}{\sigma_0^2-\sigma_1^2}(2Nln\frac{\sigma_0}{\sigma_1} - \ln\theta) = \gamma' \quad \text{for } \sigma_1^2 < \sigma_0^2 \tag{10}$$

where θ, γ and γ' are thresholds. Therefore, for the above-described binary hypothesis-testing problem, the ***sufficient statistic*** is the sum of the squares of the observations, i.e.:

$$l(\mathbf{Z}) = \sum_{i=1}^{N} Z_i^2 \tag{11}$$

The sufficient statistic Eq. (11) has also been derived in [3] and is in agreement with the analysis on grey levels transforms carried out in [7].

Let us now suppose that the signal m_1 under hypothesis H_1 is an unknown non-random parameter and that it is not known if it is smaller than or greater than m_0, which is assumed to be constant. It is obvious that in this case the best test would be that in which the value of m_1 would be measured correctly. Then, the optimum likelihood ratio test would be designed. If an actual test's performance comes close to the performance of the best (hypothetical) test outlined above, such a test will be called ***uniformly most powerful*** (UMP). The question of the existence or not of a UMP test has to be addressed. It is known [22, pp. 91] that a UMP test exists if the likelihood ratio test for every m_1 can be completely defined (including threshold) without knowledge of m_1. The following conclusions can be drawn:

1. If m_1 can take values only greater than m_0, a UMP test always exist, i.e., Eq. (9).
2. If m_1 can take values only smaller than m_0, a UMP test always exist, i.e., Eq. (10).
3. If m_1 can take values both greater than or smaller than m_0, a UMP test does not exist.

2.2 Receiver operating characteristic

Let R_0 be the decision region under the hypothesis H_0 and R_1 the corresponding decision region under the alternative hypothesis. The probability of ***false alarm*** and the probability of ***detection*** are given by:

$$P_F = \int_{R_1} f_{\mathbf{Z}|H_0}(\mathbf{Z}|H_0)d\mathbf{Z} \tag{12}$$

$$P_D = \int_{R_1} f_{\mathbf{Z}|H_1}(\mathbf{Z}|H_1)d\mathbf{Z} \tag{13}$$

The plot of P_D versus P_F for various γ as varying parameter is defined as the *receiver operating characteristic.* In the following, the probabilities of false alarm and detection will be derived theoretically for both the rules Eqs. (9,10).

The decision rule Eq. (9) has the following form:

$$l(\mathbf{Z}) = \sum_{i=1}^{N} Z_i^2 \underset{H_0}{\overset{H_1}{\gtrless}} \gamma \tag{14}$$

The threshold γ can be rewritten as:

$$\gamma = \frac{2d^2\sigma_0^2}{d^2-1}(\ln\theta + 2N\ln d) \tag{15}$$

where $d = \sigma_1/\sigma_0$. In this case, the definitions (Eqs. 12, 13) lead to the following equations:

$$P_F = Pr[\sum_{i=1}^{N} Z_i^2 \geq \gamma | H_0] \tag{16}$$

$$P_D = Pr[\sum_{i=1}^{N} Z_i^2 \geq \gamma | H_1] \tag{17}$$

Therefore, the pdf of the r.v. $w = \sum_{i=1}^{N} z_i^2$ must be evaluated if z_i are distributed according to the Rayleigh distribution with parameter σ. We maintain that:

Lemma 2 *The pdf of the r.v.* $w = \sum_{i=1}^{N} z_i^2$ *is given by:*

$$f_w(W) = \frac{W^{N-1}}{2^N\sigma^{2N}(N-1)!}\exp[-\frac{W}{2\sigma^2}] \tag{18}$$

when z_i *are distributed according to the Rayleigh distribution with parameter* σ.

The proof of Lemma 2 is given in Appendix A. By using Eq. (18), the probability of false alarm is given by:

$$P_F = \int_{\frac{\gamma}{2\sigma_0^2}}^{\infty} \frac{\xi^{N-1}}{(N-1)!}\exp(-\xi)d\xi = 1 - \mathcal{I}_\Gamma(\frac{\gamma}{2\sigma_0^2\sqrt{N}}, N-1), \quad d \geq 1 \tag{19}$$

where $\mathcal{I}_\Gamma(u, M)$ is the incomplete Gamma function defined as follows:

$$\mathcal{I}_\Gamma(u, M) \triangleq \int_0^{u\sqrt{M+1}} \frac{x^M}{M!}\exp(-x)dx \tag{20}$$

It can also be proven that:

$$P_D = 1 - \mathcal{I}_\Gamma(\frac{\gamma}{2d^2\sigma_0^2\sqrt{N}}, N-1), \quad d \geq 1 \tag{21}$$

From Eqs. (19), (21) and (15), it can be seen that the probabilities of false alarm and detection are independent of σ_0. Similarly, it can be shown that the probabilities P_F

and P_D for Eq. (10) which has the form:

$$l(\mathbf{Z}) = \sum_{i=1}^{N} Z_i^2 \underset{H_0}{\overset{H_1}{\lessgtr}} \gamma' \tag{22}$$

are given by:

$$P_F = \mathcal{I}_\Gamma(\frac{\gamma'}{2\sigma_0^2\sqrt{N}}, N-1), \quad d < 1 \tag{23}$$

$$P_D = \mathcal{I}_\Gamma(\frac{\gamma'}{2d^2\sigma_0^2\sqrt{N}}, N-1), \quad d < 1 \tag{24}$$

The receiver operating characteristics for some representative values of N and d are plotted in figure 1. Figure 1a shows how the shape of the receiver operating characteristic is changed for $d = 0.8912, 0.7943, 0.707$ keeping N equal to 9. Figure 1b shows the corresponding receiver operating characteristics for the reciprocal values of d used in Figure 1a for the same value of N. As expected, the receiver operating characteristic becomes superior as d decreases when $d < 1$ (or increases when $d > 1$). The effect of increasing N while keeping d equal to $\sqrt{2}$ is shown in figure 1c. Again, the receiver operating characteristic becomes better with the increase of the length N.

3 ESTIMATION OF A CONSTANT SIGNAL FROM SPECKLE

In this section, we estimate the parameter m in Eq. (1) if n is multiplicative noise independent of m which is distributed as follows:

$$f_n(\mathcal{N}) = \frac{\pi\mathcal{N}}{2}\exp[-\frac{\pi\mathcal{N}^2}{4}] \quad \mathcal{N} > 0 \tag{25}$$

We shall examine the maximum likelihood estimator and the L-estimator of the constant signal.

3.1 ML-Estimator of the Constant Signal

The conditional density function of the observations assuming that $m = M$ is given by [21]:

$$f_{z|m}(Z|M) = \frac{1}{M} f_n(\frac{Z}{M}) \quad M > 0 \tag{26}$$

Let us suppose that we have a set of N observations. Then:

$$f_{\mathbf{Z}|m}(\mathbf{Z}|M) = \frac{\pi^N}{2^N M^{2N}} \prod_{i=1}^{N} Z_i \exp[-\frac{\pi Z_i^2}{4M^2}] \tag{27}$$

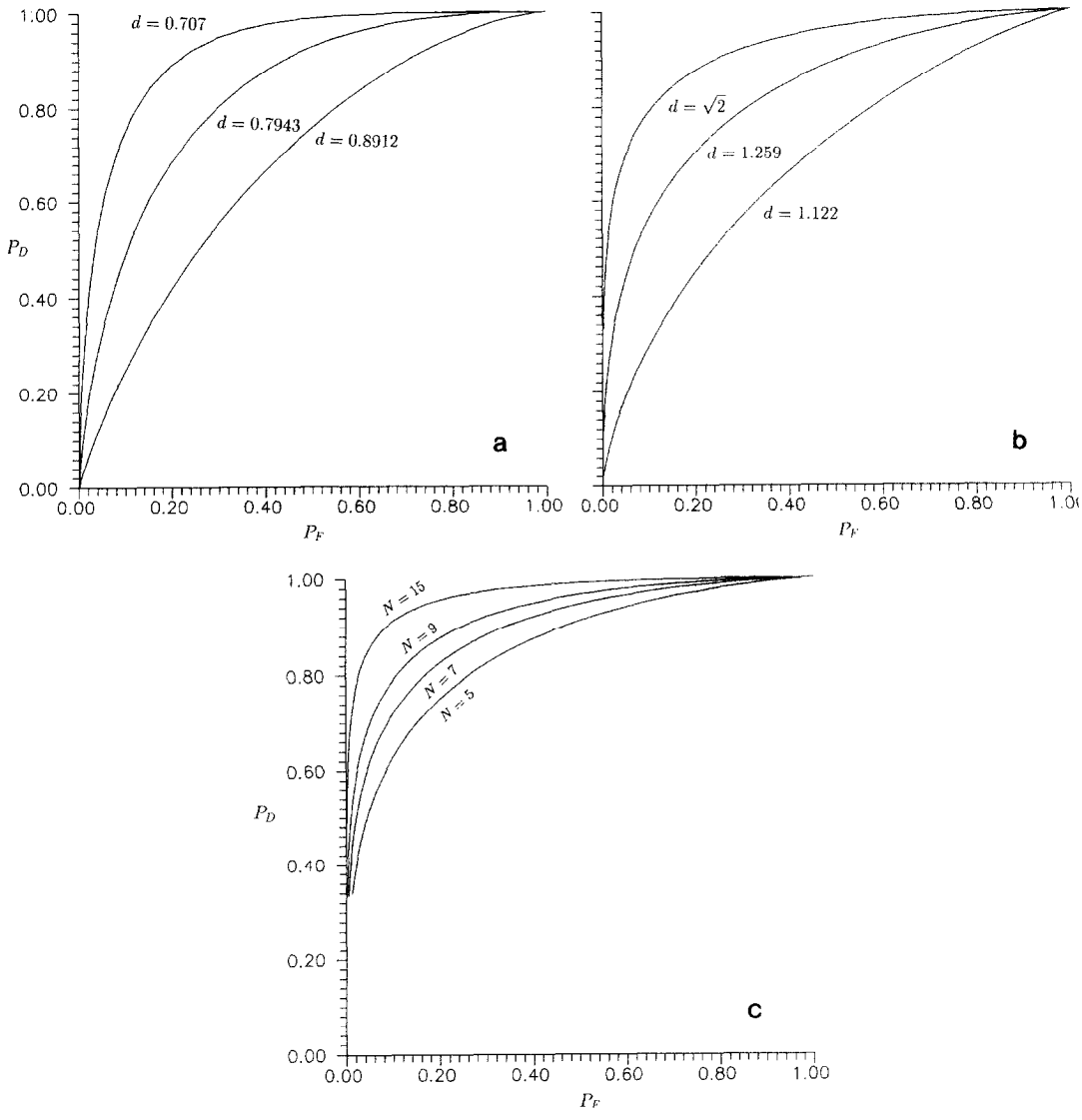

Fig. 1 Receiver Operating Characteristic: Rayleigh random variables with unequal means (a) for $d < 1$ and $N = 9$; (b) for $d > 1$ and $N = 9$; (c) for $d = \sqrt{2}$ and N variable.

or equivalently:

$$\ln f_{\mathbf{Z}|m}(\mathbf{Z}|M) = N ln\frac{\pi}{2} + \sum_{i=1}^{N} \ln Z_i - 2N \ln M - \frac{\pi}{M^2} \sum_{i=1}^{N} Z_i^2 \tag{28}$$

The ML-estimate of M maximizes the log-likelihood function $\ln f_{\mathbf{Z}|m}(\mathbf{Z}|M)$, i.e.,

$$\frac{\partial}{\partial M} \ln f_{\mathbf{Z}|m}(\mathbf{Z}|M)|_{M=\hat{m}_{ML}(\mathbf{Z})} = 0 \tag{29}$$

The solution of Eq. (29) is given by:

$$\hat{m}_{ML} = \frac{\sqrt{\pi}}{2}\sqrt{\frac{1}{N}\sum_{i=1}^{N} Z_i^2} \tag{30}$$

Therefore, it has been proven that the ML-estimator of the constant signal is the L_2 mean [19] scaled by the factor $\frac{\sqrt{\pi}}{2}$. Since the ML-estimate commutes over nonlinear operations [22], if the envelope-detected ultrasound signal is log-compressed, i.e.,

$$y = \ln z \tag{31}$$

then the ML-estimate of the constant signal will be:

$$\hat{m}_{ML} = \frac{\sqrt{\pi}}{2}\sqrt{\frac{1}{N}\sum_{i=1}^{N} \exp[2Y_i]} \tag{32}$$

In the following, the expected value and the variance of the ML-estimator as well as the mean-squared estimation error will be evaluated. We maintain that:

Lemma 3 *Let $\pi(N)$ be the following polynomial of N:*

$$\pi(N) \triangleq \frac{\Gamma[N+\frac{1}{2}]}{\sqrt{N}(N-1)!} \tag{33}$$

The expected value of the ML-estimator is:

$$\mathrm{E}[\hat{m}] = \pi(N)M \tag{34}$$

its variance is given by:

$$\mathrm{var}[\hat{m}] = (1-\pi^2(N))M^2 \tag{35}$$

and the mean-squared estimation error is:

$$\mathrm{E}[(\hat{m}-M)^2] = 2\,(1-\pi(N))M^2 \tag{36}$$

The proof of the Lemma 3 can be found in Appendix B. The terms $\pi(N)$ and $[1-\pi^2(N)]$ are plotted for various values of the filter length N in figure 2. It can be seen that the expected value of the estimator is very close to M for $N > 10$. Also, the variance of the estimator as well as the mean-squared estimation error vanishes for large number of observations N. Furthermore, the following asymptotic properties of the ML-estimate also hold [22]:

1. The ML-estimate is consistent, i.e., the solution of Eq. (29) converges in probability to the correct value.

2. The ML-estimate is asymptotically efficient, i.e.,

$$\lim_{N\to\infty} \frac{\mathrm{var}[\hat{m}_{ML}(\mathbf{z}) - M]}{(-\mathrm{E}[\frac{\partial^2 \ln f_{\mathbf{Z}|m}(\mathbf{Z}|M)}{\partial M^2}])^{-1}} = 1 \tag{37}$$

3.2 Optimal L-Estimator of the Constant Signal

Another class of estimators found extensive applications in digital signal and image processing are the L-estimators which are based on the order statistics. We have chosen the L-estimators for estimating the constant signal for three reasons:

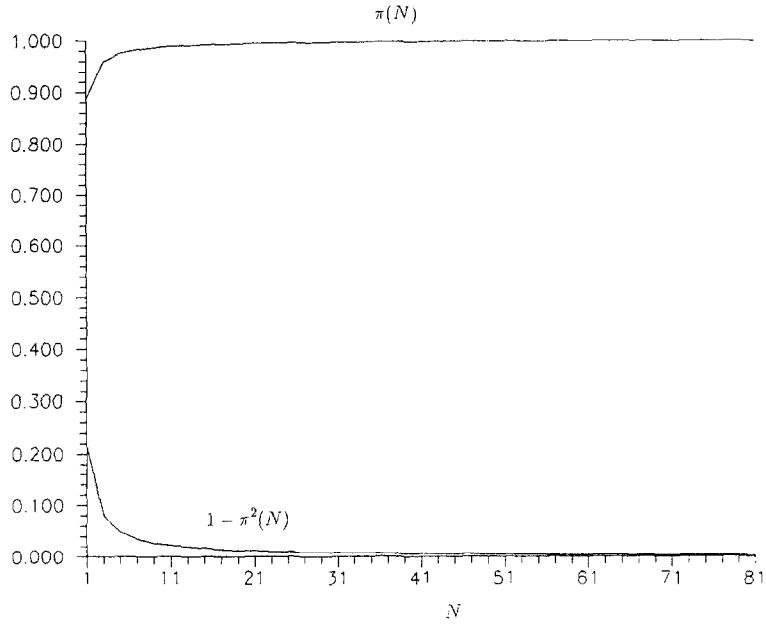

Fig. 2 Plot of the terms $\pi(N)$ and $1-\pi^2(N)$ versus N.

1. L-estimators are a large class of robust estimators related to the ML-estimators [15].
2. There is a well-defined method for their design as minimum mean-squared-error estimators of location.
3. The corresponding mean square error is always less or equal to that produced by the arithmetic mean.

The output of the L-estimator of length N is given by:

$$y(k) = \mathbf{a}^T \mathbf{z}_r(k) \tag{38}$$

where $\mathbf{a} = (a_1, a_2, \ldots, a_N)^T$ is the L-estimator coefficient vector and $\mathbf{z}_r(k) = (z^k_{(1)}, z^k_{(2)}, \ldots, z^k_{(N)})^T$ is the vector of the observations arranged in ascending order of magnitude (i.e., order statistics). We shall design the L-estimator which minimizes the mean-squared-error (MSE) $\mathrm{E}[(y(k)-m)^2]$ under the constraint of unbiased estimation for the model Eq. (1). The unbiasedness condition implies that the L-estimator output will converge to the estimated constant signal in an ensemble-average sense. Therefore, the following equation is satisfied:

$$\mathrm{E}[y(k)] = m \Leftrightarrow \sum_{i=1}^{N} a_i \mathrm{E}[n^k_{(i)}] = 1 \tag{39}$$

or in vector notation:

$$\mathbf{a}^T \overline{\mu} = 1 \tag{40}$$

where $\overline{\mu} = (\mathrm{E}[n_{(1)}], \mathrm{E}[n_{(2)}], \ldots, \mathrm{E}[n_{(N)}])^T$ is the vector of the expected values of the order statistics. The superscript k is dropped out due to stationarity. Let $\mathbf{n}_r = (n_{(1)}, n_{(2)}, \ldots, n_{(N)})^T$ be the vector of the ordered noise samples and $\mathbf{R} = \mathrm{E}[\mathbf{n}_r \mathbf{n}_r^T]$ be the correlation matrix of the ordered noise samples. The MSE is given by:

$$\mathrm{MSE} = m^2(\mathbf{a}^T\mathbf{R}\mathbf{a} - 1) \tag{41}$$

The L-estimator coefficient vector $\mathbf{a}$ which minimizes Eq. (41) under Eq. (40) is given by:

$$\mathbf{a} = \frac{\mathbf{R}^{-1}\overline{\mu}}{\overline{\mu}^T\mathbf{R}^{-1}\overline{\mu}} \tag{42}$$

In order to calculate $\mathbf{a}$, we need matrix $\mathbf{R}$ whose elements are moments of the order statistics. Therefore, we have to evaluate the moments of the order statistics for the Rayleigh distribution with parameter σ. In our case, the parameter σ equals $\sqrt{2/\pi}$, as can be seen from Eq. (25). The following lemma will enable us to evaluate numerically the elements of the correlation matrix $\mathbf{R}$ by using the Gauss-Legendre quadrature formula in a computationally efficient manner:

Lemma 4 *The diagonal elements of the correlation matrix* $\mathbf{R}$ *are given by:*

$$R_{ii} = \mathrm{E}[n_{(i)}^2] = 2\sigma^2 \frac{N!}{(i-1)!\,(N-i)!} \int_0^1 (-\ln\xi)\, \xi^{N-i}(1-\xi)^{i-1} d\xi \quad i = 1, \ldots, N \tag{43}$$

Furthermore, the off-diagonal elements can be evaluated by:

$$\begin{aligned} R_{ij} &= \mathrm{E}[n_{(i)}n_{(j)}] = \sigma^2 \frac{N!}{(i-1)!\,(j-i-1)!\,(N-j)!} \int_0^1 \int_0^\alpha \sqrt{-2\ln\alpha}\, \alpha^{j-i-1}\,(1-a)^{i-1} \\ &\times \sqrt{-2\ln\beta}\,(1-\frac{\beta}{\alpha})^{j-i-1}\,\beta^{N-j}\, d\alpha\, d\beta \qquad 1 \le i < j \le N \end{aligned} \tag{44}$$

Similarly, it can be proven that the elements of the vector $\overline{\mu}$ are given by:

$$\mu_i = \mathrm{E}[n_{(i)}] = \sigma\sqrt{2}\frac{N!}{(i-1)!\,(N-i)!} \int_0^1 \sqrt{-\ln\lambda}\,(1-\lambda)^{i-1}\lambda^{N-i}\, d\lambda \tag{45}$$

The L-estimator coefficients are shown in figure 3 for various L-estimator lengths N. It can be seen that the higher order statistics are weighted by larger coefficients in all cases. It is also recognized an almost linear increase in the magnitude of the L-estimator coefficients $\mathbf{a}$ with the order number i. There is a tight connection between the ML-estimator derived previously and the L-estimator because the ML-estimate (i.e., the L_2 mean) is always larger than that of the arithmetic mean and smaller than the maximal observation [23]. Therefore, the higher order statistics play more significant role than the smaller ones in the ML-estimator, too.

4 GENERALIZATION TO A RANDOM LESION SIGNAL

In most practical cases, it is unrealistic to consider a constant signal hypothesis. Without any loss of generality, the following binary hypothesis problem will be assumed:

$$\begin{aligned} H_1 : z &= mn \\ H_0 : z &= n \end{aligned} \tag{46}$$

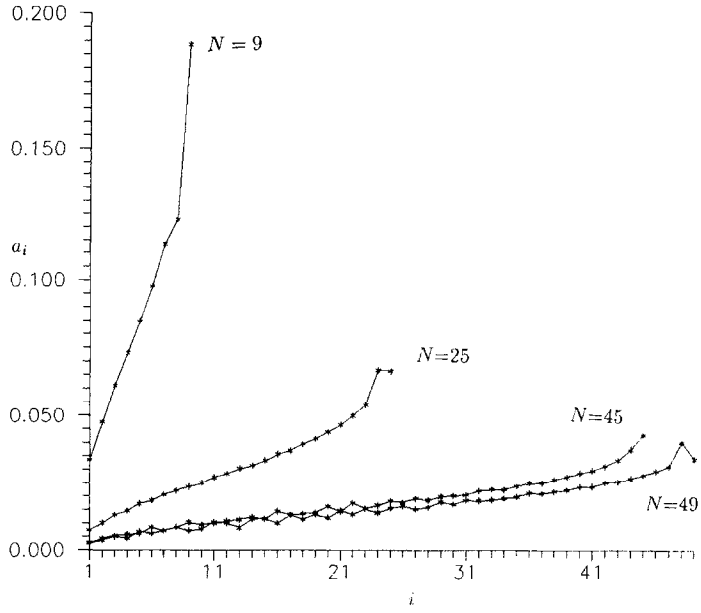

Fig. 3 L-estimator coefficients for various lengths N.

where m, n are random variables. Our aim is to perform detection and estimation based on this model. Since m is a r.v., the conditional density of the observations assuming H_1 is given by:

$$f_{z|H_1}(Z|H_1) = \int_{\chi_m} f_{z|m,H_1}(Z|M, H_1) \; f_{m|H_1}(M|H_1)dM \tag{47}$$

where χ_m is the domain of the r.v. m. The following assumptions are made:

1. n is a Rayleigh r.v. having unity expected value and variance $\frac{4-\pi}{\pi}$, i.e., its pdf is given by Eq. (25).

2. The conditional density of the observations under the hypothesis H_1 and the condition that m is known is given by:

$$f_{z|m,H_1}(Z|M, H_1) = \frac{1}{M} f_n(\frac{Z}{M}) = \frac{\pi Z}{2M^2} \exp(-\frac{\pi Z^2}{4M^2}) \;\; M > 0 \tag{48}$$

3. The conditional density of m assuming H_1 must be chosen in such a way that it represents a realistic model and it is mathematically tractable. A Maxwell density with parameter Λ fulfills both requirements. Thus:

$$f_{m|H_1}(M|H_1) = \frac{M^2 \exp(-\Lambda M^2)}{K} \tag{49}$$

The following equation must be satisfied so that Eq. (49) to be pdf:

$$\int_0^\infty f_{m|H_1}(M|H_1)dM = 1 \tag{50}$$

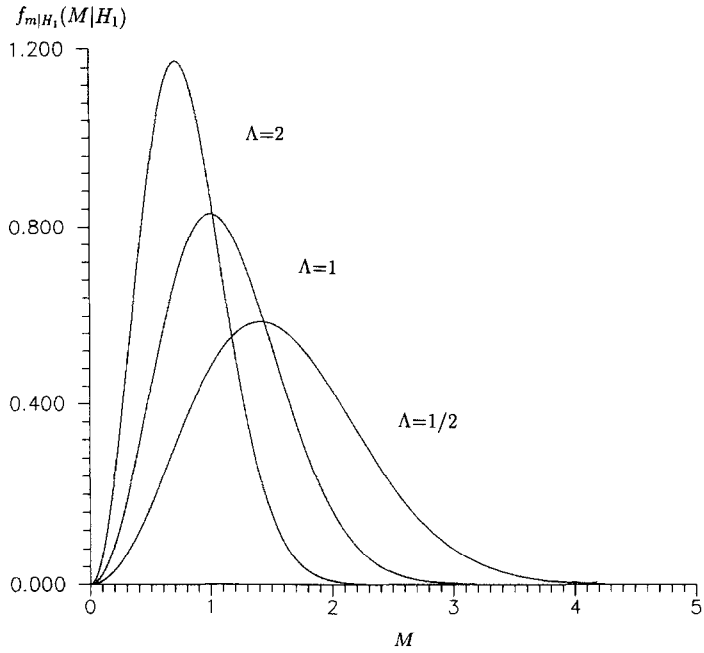

Fig. 4 Plot of Maxwell probability density function for $\Lambda = 1/2, 1, 2$.

Therefore, the constant K is given by:

$$K = \frac{\sqrt{\pi}}{4\Lambda^{3/2}} \tag{51}$$

A plot of Maxwell pdf for $\Lambda = 1/2, 1, 2$ is shown in figure 4. By substituting Eqs. (49) and (51) in Eq. (47), we obtain:

$$f_{z|H_1}(Z|H_1) = \pi\Lambda Z \exp(-Z\sqrt{\Lambda\pi}) \tag{52}$$

It can be seen that the resulted density is a Gamma density. Such a result is very reasonable, because it is known that speckle can be modeled by a Gamma density function [15, pp. 226]. Based on N observations the log-likelihood test leads to:

$$\sum_{i=1}^{N} Z_i^2 - 4\sqrt{\frac{\Lambda}{\pi}} \sum_{i=1}^{N} Z_i \underset{H_0}{\overset{H_1}{\gtrless}} \frac{4}{\pi}(\theta - N \ln 2\Lambda) = \gamma'' \tag{53}$$

The problem of the estimation of the signal m will be treated next. The (MAP) estimate of the signal is defined by:

$$\frac{\partial}{\partial M} f_{m|\mathbf{z}}(M|\mathbf{Z})|_{M=\hat{m}_{MAP}(\mathbf{z})} = 0 \tag{54}$$

By applying the Bayes theorem, we have:

$$f_{m|\mathbf{z}}(M|\mathbf{Z}) = q(\mathbf{Z})\frac{1}{M^{2N-2}}\exp[-(\Lambda M^2 + \frac{\pi}{4M^2}\sum_{i=1}^{N} Z_i^2)] \tag{55}$$

where

$$q(\mathbf{Z}) = (\frac{\pi}{2})^N \frac{4\Lambda^{3/2}}{\sqrt{\pi}} \frac{\prod_{i=1}^{N} Z_i}{f_{\mathbf{Z}}(\mathbf{Z})} \tag{56}$$

By replacing Eq. (55) in Eq. (54), we obtain:

$$(\frac{\pi}{4}\sum_{i=1}^{N} Z_i^2)\frac{1}{M^4} - (N-1)\frac{1}{M^2} - \Lambda = 0 \tag{57}$$

Therefore, the MAP estimate of the signal m is given by:

$$\hat{m}_{MAP}(\mathbf{z}) = \sqrt{\frac{\frac{\pi}{2}\sum_{i=1}^{N} Z_i^2}{(N-1) + \sqrt{(N-1)^2 + \pi\Lambda\sum_{i=1}^{N} Z_i^2}}} \tag{58}$$

It can be seen that for $\Lambda = 0$ the MAP estimate of m reduces to the form of the ML-estimate of the constant signal. Indeed:

$$\hat{m}_{MAP}(\mathbf{z}; \Lambda = 0) = \frac{\sqrt{\pi}}{2}\sqrt{\frac{1}{N-1}\sum_{i=1}^{N} Z_i^2} \tag{59}$$

5 EXPERIMENTAL RESULTS

The proposed ML-estimator and the L-estimator designed in section 3 have been applied both to simulated ultrasound B-mode images as well as to real ultrasonic images for speckle suppression. Simulated ultrasound B-mode images are used in order to evaluate the performance of various filters in speckle suppression and to select parameters (such as filter length and thresholds involved) in the image processing task. Figure 5a and 6a are simulations of an homogeneous piece of tissue (4×4 cm) with a circular lesion in the middle. The lesion has a diameter of 2 cm. These ultrasound B-mode images have been produced and described by Verhoeven et al. [24]. The lesion differs from the background in reflection strength (+3 dB). The background has a number density of scatterers of 5000/cm^3. The lesion has a number density of scatterers of either 5000/cm^3 (figure 5a) or 500/cm^3 (figure 6a). In the former case, there is no change in second order statistics between lesion and background. In the later case, the lesion is characterized by a sub-Rayleigh distribution. Both simulated image have dimensions 241×241 and resolution 6 bits/pixel. The grey level histograms of the pixels belonging to the lesion area and to the background in both images are plotted in figures 5b and 6b respectively. It can be seen that they are very similar to the Rayleigh pdf. The expected value, the variance, the SNR, i.e., the ratio of the expected value to the standard deviation and the parameter σ under each hypothesis are listed in table 1.

It has been noted that working with the correlation cell concept for intensity yields a very good approximation to the independence assumption [1,3]. Smith et al. argue

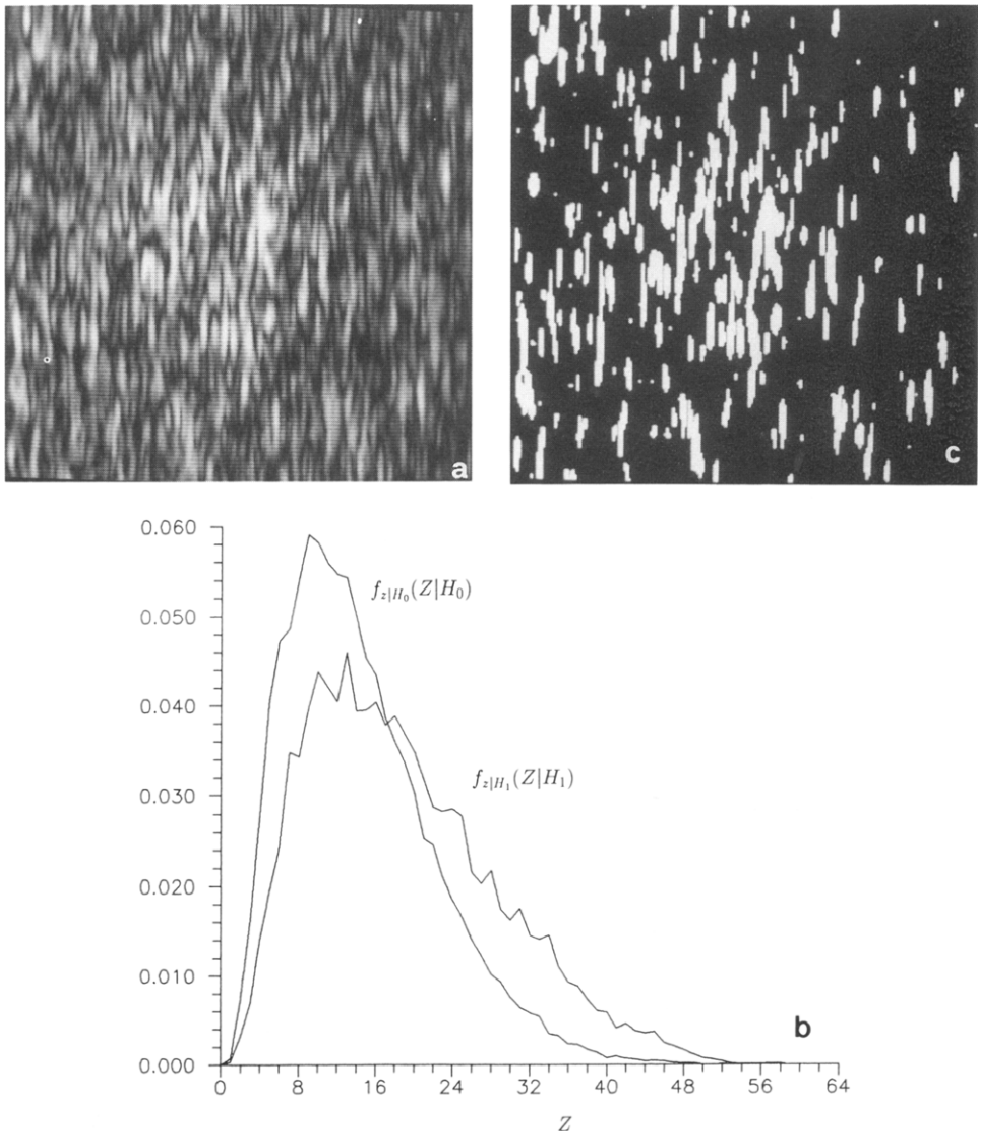

Fig. 5 (a) Simulation of an homogeneous piece of tissue with a circular lesion in the middle; lesion/background amplitude=+3 dB; Number density of scatterers in the background and the lesion 5000/cm^3; (b) grey level histograms of the pixels belonging to the lesion and to the background areas; (c) thresholded original image.

that the number of observations N must be chosen equal to the number of speckle correlation cells within the measurement area [3]. Since our purpose is to apply filters scanning the ultrasonic image in raster fashion such a recommendation cannot be used directly. We have investigated the effect of the lateral and axial correlation sizes in the

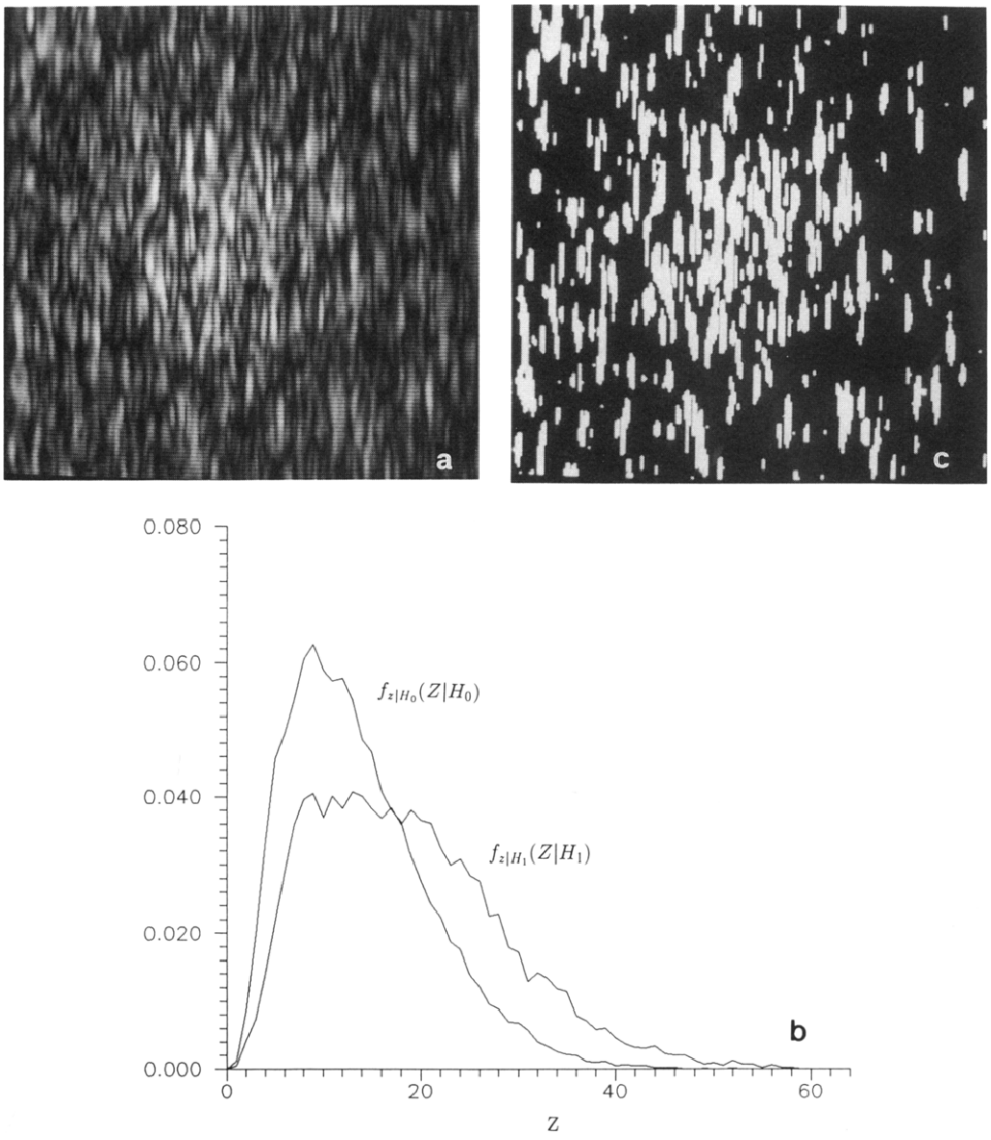

Fig. 6 (a) Simulation of an homogeneous piece of tissue with a circular lesion in the middle; lesion/background amplitude=+3 dB; Number density of scatterers in the background 5000/cm^3 and the lesion 500/cm^3; (b) grey level histogram of the pixels belonging to the lesion and to the background areas; (c) thresholded original image.

selection of filter window dimensions instead. Verhoeven et al. have found that the lateral and the axial correlation sizes for the ultrasound B-mode images used are of the order of 15 and 3 pixels respectively [24]. The lateral correlation size refers to the vertical direction, whereas the axial correlation size refers to the horizontal one. We have been employed three different types of filter window:

Table 1. Mean, variance, SNR and σ under each hypothesis for the ultrasound B-mode images shown in figures 5a and 6a

Image	Hypothesis	Mean	Variance	SNR	σ
figure 5a	H_0–background	14.38	58.86	1.875	11.4787
	H_1–lesion	18.89	96.95	1.919	15.0706
figure 6a	H_0–background	13.59	52.58	1.874	10.8448
	H_1–lesion	18.69	95.15	1.916	14.914

(i) a square window having area approximately equal to that of the speckle correlation cell, e.g., a 7×7 filter window (neglect of different lateral and axial correlation sizes),

(ii) a rectangular window having dimensions proportional to the lateral and axial correlation sizes, e.g., a 15×3 filter window,

(iii) a rectangular window having dimensions inversely proportional to the lateral and axial correlation sizes, e.g., a 3×15 filter window.

The filter window dimensions correspond to the number of rows and columns.

We have examined the success of the following strategies in lesion detectability:

1. thresholding the original image without any processing
2. filtering the original image by a median filter and thresholding the filtered image
3. filtering the original image by an arithmetic mean filter and thresholding the filtered image
4. filtering the original image by the ML-estimator of the constant signal and thresholding the filtered image
5. filtering the original image by L-estimator and thresholding the filtered image.

In the processing of ultrasound B-mode images, we have used all the types of windows outlined above. We have compared the performance of the above-described strategies using as figures of merit the area under the ROC in each case and the probability of detection P_D for a threshold chosen so that the probability of false alarm P_F to be $\simeq 10\%$. The area under the ROC corresponds to the fraction of the correct enforced answers when we detect the signal in two stimuli and know that the signal exists only in one of them [8] . As has been noted in [6], a comparison based on the probability of detection P_D for a fixed probability of false alarm P_F holds only for this operating point and is sometimes an inadequate figure of merit, especially when ROC curves cross. Wagner recommends the area under the ROC as a more reliable figure of merit for a complete characterization of the whole ROC curve. Some experimental evaluations of

Table 2. Figures of merit for lesion detection on the simulated ultrasound B-mode image of figure 5a

Method	P_F %	P_D %	Threshold	$\hat{P}_D$ %	Area under ROC
Image	9.4638	23.7045	26	25.1064	0.628564
Thresholding	11.1526	26.486	25		
Median	9.1178	28.1779	22	30.2125	0.693291
7×7	11.7239	32.6070	21		
ar. mean	7.7749	27.2035	22	32.3480	0.717286
7×7	10.4516	32.6247	21		
ML-estimator	10.3150	33.0942	20	33.0942	0.722967
7×7					
L-estimator	9.5161	31.8806	20	33.4472	0.724172
7×7	13.0485	38.8077	19		
Median	8.3768	24.0322	24	25.776	0.673532
15×3	10.1573	27.3275	23		
ar. mean	8.6375	25.5381	23	26.89	0.686538
15×3	10.6066	29.4269	22		
ML-estimator	9.3194	28.2665	21	28.2665	0.692902
15×3					
L-estimator	8.2930	26.6454	21	28.8606	0.696022
15×3	10.4273	31.2517	20		
Median	8.7026	34.5203	20	34.8972	0.728730
3×15	12.3475	42.0852	19		
ar. mean	7.5761	37.8333	20	40.6348	0.767549
3×15	11.7098	46.6826	19		
ML-estimator	8.8842	41.6866	19	41.6866	0.773853
3×15					
L-estimator	8.4326	40.5350	19	41.4017	0.774033
3×15	13.5695	50.3942	18		

these figures of merit for both images shown in figures 5a and 6a are given in tables 2 and 3 respectively. We have also included in tables 2 and 3 a column having entries probabilities of detection $\hat{P}_D$ obtained by linear interpolation between the closest experimental values to a reference probability of false alarm in all methods. In the case of figure 5a, a probability of false alarm close to 10% for the ML-estimator has been used as reference. In the case of figure 6a, a probability of false alarm close to 10% for the arithmetic mean filter has been used as reference. All comparisons between the probabilities of detection have been carried out by using $\hat{P}_D$.

It is seen that the selection of the filter window dimensions plays an important role in the results obtained. By selecting a square window that approximately has the same area with the speckle correlation cell, we have obtained almost identical

Table 3. Figures of merit for lesion detection on the simulated ultrasound B-mode image of figure 6a

Method	P_F %	P_D %	Threshold	$\hat{P}_D$ %	Area under ROC
Image	8.7306	25.8216	25	27.81	0.650363
Thresholding	10.5517	28.9042	24		
Median	8.7335	34.5912	21	37.2554	0.732352
7×7	11.1958	40.1896	20		
ar. mean	9.9053	39.3392	20	39.3392	0.756338
7×7					
ML-estimator	9.9008	40.4553	19	40.712	0.765246
7×7	13.5288	47.161	18		
L-estimator	9.2271	39.0291	19	40.3488	0.767360
7×7	12.7822	45.9474	18		
Median	9.6802	30.7733	22	34.095	0.699571
15×3	11.8029	34.9898	21		
ar. mean	10.1131	33.6257	21	33.6257	0.716538
15×3					
ML-estimator	8.975	31.7211	20	34.218	0.725847
15×3	11.3118	36.85	19		
L-estimator	7.9392	29.5597	20	34.6	0.729507
15×3	10.3831	34.8127	19		
Median	8.7608	42.2447	19	47.913	0.780025
3×15	12.6408	49.2338	18		
ar. mean	11.9076	54.7701	18	54.7701	0.819013
3×15					
ML-estimator	9.0378	51.2357	18	56.342	0.829192
3×15	14.6285	61.1835	17		
L-estimator	8.6375	50.3322	18	56.336	0.830014
3×15	14.0839	60.3331	17		

results with a rectangular window with dimensions proportional to the lateral and axial correlation sizes. The best results are obtained for filter window dimensions being inversely proportional to the lateral and axial correlation sizes. In the later case, an increase of 10% in the area under the ROC as well as in the probability of detection has been obtained for all filtering methods. This is attributed to the fact that more speckle cells fall into the filter window, thus producing better noise suppression. However, it must be noted that using window sizes inversely proportional to the speckle correlation cell may enhance edge and image detail blurring in real ultrasonic images.

It can be seen that the proposed nonlinear filters are relatively better than the median and arithmetic mean with respect to the area under the ROC and the probability of detection for the same probability of false alarm. It is clear that the median filter

is inappropriate for speckle suppression because the area under its ROC is always less than that of the arithmetic mean, the ML-estimator and the L-estimator. In the sequel, the performance of the proposed nonlinear filters is examined in comparison to the arithmetic mean. By inspecting tables 2 and 3, it can be verified that the L-estimator is superior than the ML-estimator and the arithmetic mean of the same dimensions with respect to the area under the ROC. It has been noticed that the area under the ROC of the L-estimator is greater than the corresponding one of the arithmetic mean for about 0.65%–1.3%. On the other hand, it is found that the ML-estimator is the most efficient method for the half number of tests performed with respect to the probability of detection. The L-estimator gives the best results for the rest of them. An almost 2% higher probability of detection is obtained by using the ML-estimator instead of the arithmetic mean. The corresponding highest probability of detection for the L-estimator is about 1.6% higher than the one obtained by the arithmetic mean. Similar results have also been obtained when the amplitude of the reflections in the lesion are weaker than the reflection strength in the background.

The thresholded images (figures 5a and 6a) are shown in figures 5c and 6c respectively. Pixels classified as lesion are shown white. It can be clearly seen that the image thresholding itself is inadequate to detect correctly the lesion. Figures 7a,b show the output of the 15×3 ML-estimator applied to figure 5a and the result of thresholding respectively. In figures 8a,b it can also be seen the filtered image of figure 5a by the 15×3 L-estimator and the result of thresholding. The same threshold 21 has been used in both cases. Figures 9a,b show the output of the 3×15 ML-estimator applied to figure 6a and the result of thresholding respectively. The filtered image (figure 6a) by the 3×15 L-estimator and the result of thresholding are shown in figures 10a,b. A threshold equal to 17 has been used in both cases. It must be noted that similar results to those presented in figures 9 and 10 have also been obtained for the ultrasound B-mode image of figure 5a when the ML-estimator and the L-estimator of dimensions 3×15 have been employed.

We have applied the proposed nonlinear filters to several real ultrasonic images. A representative real ultrasonic image of liver recorded using 3 MHz probe shown in figure 11a. The output of the ML-estimator and L-estimator, all of dimensions 5×5, are shown in figures 11b,c. It is seen that the proposed nonlinear filters suppress the speckle noise effectively. However, any spatial filtering without adjusting its smoothing performance at each point of the image according to the local image content results in edge blurring. Better edge preservation is attained by the so-called signal-adaptive filters [15]. Based on the optimality of the proposed nonlinear filters studied in this paper, signal-adaptive ML-filters as well as signal adaptive L-filters can be designed to solve the above-mentioned problem. This topic is currently being investigated. Preliminary encouraging results have recently been reported [25].

6 CONCLUSIONS

The detection and estimation of a lesion signal in ultrasound B-mode images has been treated thoroughly. Optimal decision rules have been derived both in the case

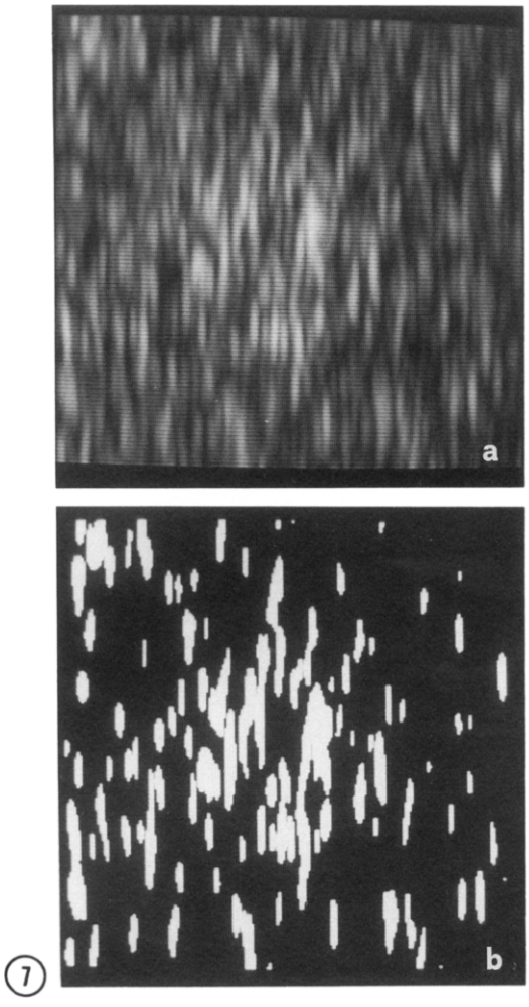

7

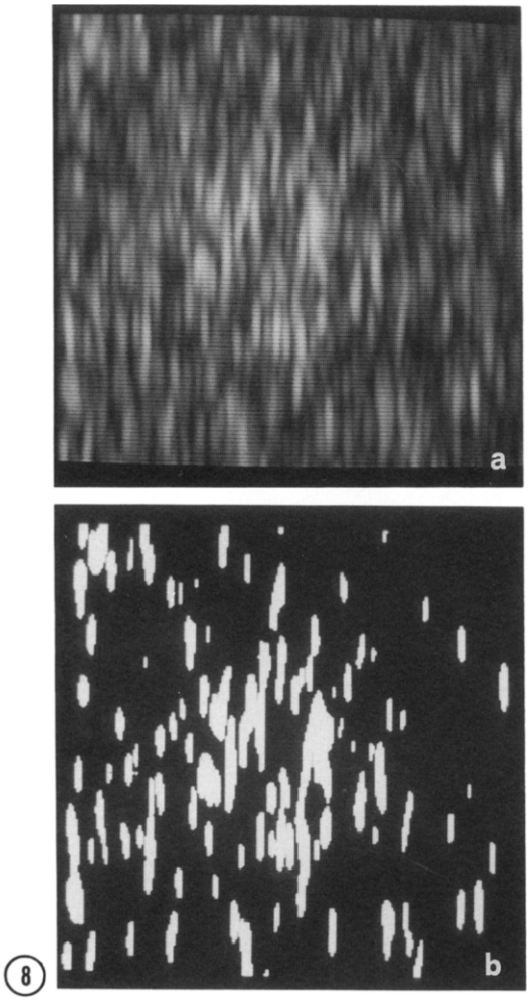

8

Fig. 7 (a) Output of the 15×3 ML-estimator applied to figure 5a; (b) Result of thresholding.

Fig. 8 (a) Output of the 15×3 L-estimator applied to figure 5a; (b) Result of thresholding.

of a constant signal as well as in the case of a random lesion signal. In the first case, the probabilities of false alarm and detection have been evaluated theoretically. The ML-estimator and the L-estimator for estimating a constant signal from speckle have been designed. The MAP estimate of the lesion signal has also been found under the assumption that the lesion signal is distributed according to the Maxwell distribution. The use of the ML-estimator and the L-estimator has been proposed for speckle suppression. It has been verified by simulations that both these filters are better than the arithmetic mean filter in lesion detection. The figures of merit used are the area

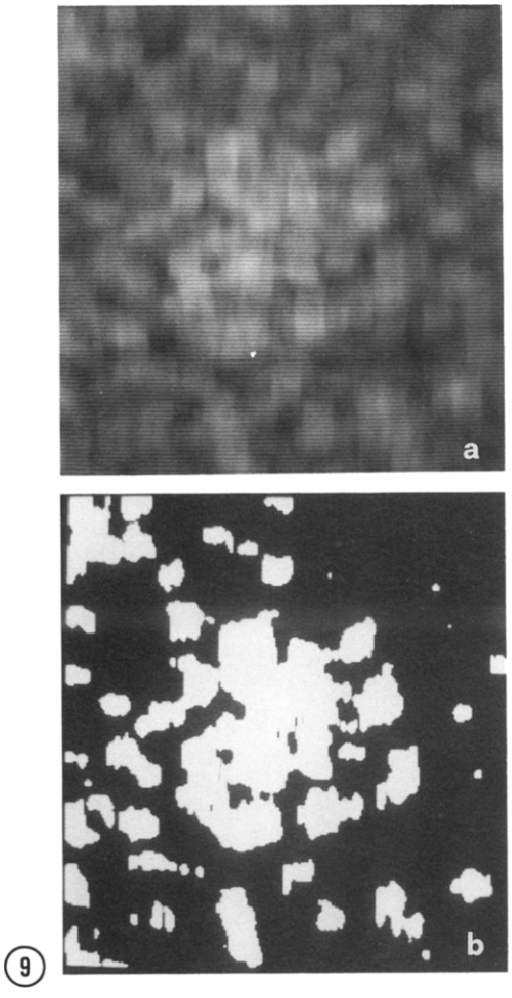

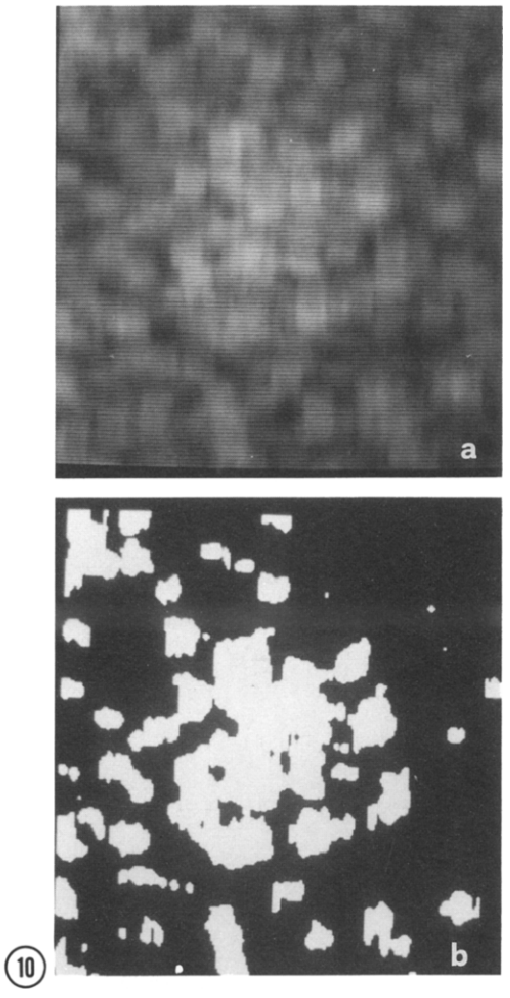

Fig. 9 (a) Output of the 3×15 ML-estimator applied to figure 6a; (b) Result of thresholding.

Fig. 10 (a) Output of the 3×15 L-estimator applied to figure 6a; (b) Result of thresholding.

under the ROC and the probability of detection for fixed probability of false alarm. The performance of the proposed filters can be further enhanced by using a measure of local signal activity that will enable space-varying processing and thus will take into account the local image content. Signal-adaptivity can be combined with region segmentation, so that the filter can perform differently in the various image regions. Neural networks can be used for ultrasonic region segmentation. This approach which leads to a signal-adaptive ML-estimator or L-estimator currently is a subject of ongoing research.

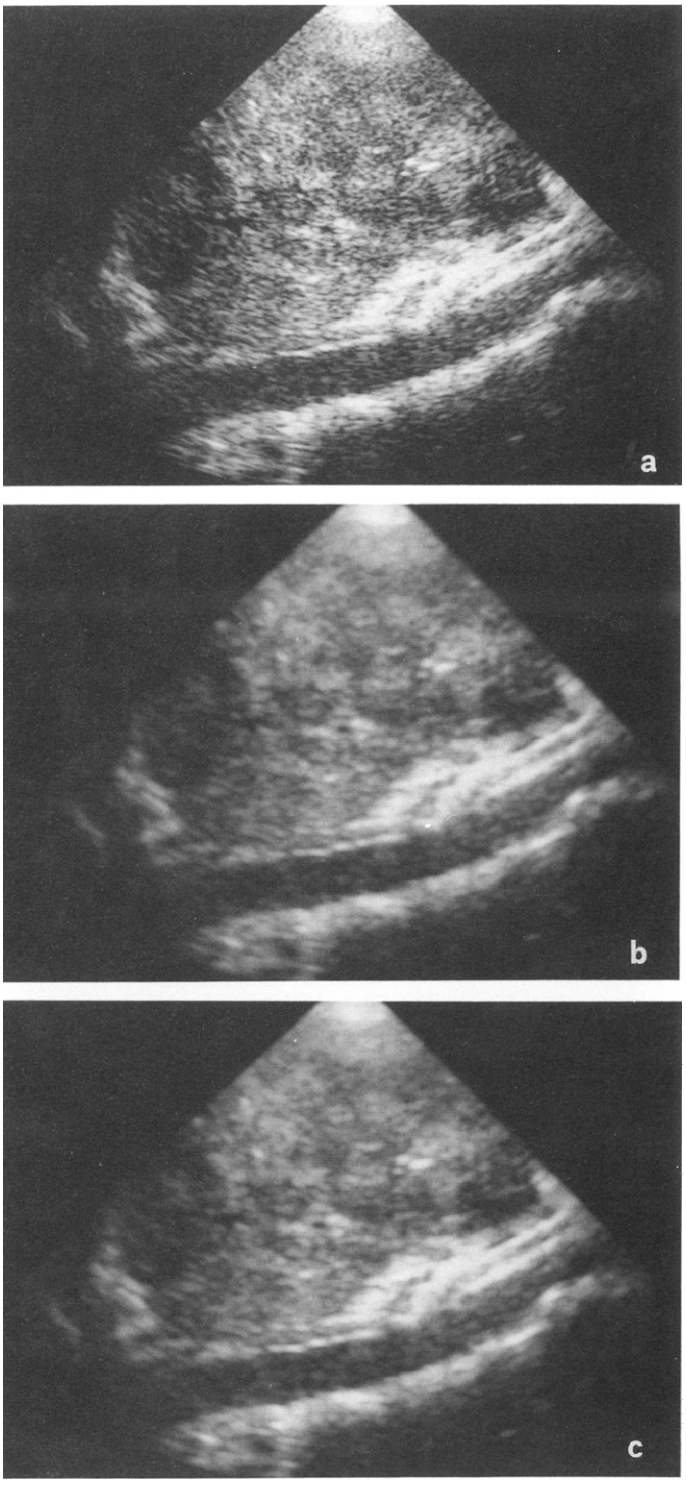

Fig. 11 (a) Real ultrasound image of liver recorded using 3 MHz probe; (b) Output of the 5×5 ML-estimator; (c) Output of the 5×5 L-estimator.

Appendix A

Proof of Lemma 2

The joint pdf of z_i is given by:

$$f_{\mathbf{z}}(\mathbf{Z}) = \frac{\prod_{i=1}^{N} Z_i}{\sigma^{2N}} \exp[-\frac{\mathbf{Z}^T\mathbf{Z}}{2\sigma^2}] \qquad (A-1)$$

where $\mathbf{Z} = (Z_1, Z_2, \ldots, Z_N)^T$. Let $\mathbf{y} = (y_1, y_2, \ldots, y_N)^T$. By making the following random variable transformation:

$$\begin{aligned} w = y_1 &= \mathbf{z}^T\mathbf{z} \\ y_2 &= z_1 \\ &\vdots \\ y_N &= z_{N-1} \end{aligned} \qquad (A\text{-}2)$$

we obtain:

$$f_{\mathbf{y}}(\mathbf{Y}) = \frac{\prod_{i=2}^{N} Y_i}{\sigma^{2N}} \exp[-\frac{Y_1}{2\sigma^2}] \qquad (A-3)$$

Therefore:

$$f_w(W) = \frac{1}{2\sigma^{2N}} \exp[-\frac{W}{2\sigma^{2N}}] \overbrace{\int\int\cdots\int_{\mathcal{J}}}^{N-1} Y_2 Y_3 \cdots Y_N \; dY_2 dY_3 \cdots dY_N \qquad (A-4)$$

where $\mathcal{J}$ is the region of integration defined by the set of the following $N-1$ inequalities:

$$\begin{aligned} 0 < Y_N &< \sqrt{W - (Y_2^2 + \cdots + Y_{N-1}^2)} \\ 0 < Y_{N-1} &< \sqrt{W - (Y_2^2 + \cdots + Y_{N-2}^2)} \\ &\vdots \\ 0 < Y_2 &< \sqrt{W} \end{aligned} \qquad (A\text{-}5)$$

Carrying out the integration over $\mathcal{J}$ (18) results. □

Appendix B

Proof of Lemma 3

It can be easily proven by using Eq. (18) that the pdf of the r.v. x defined by:

$$x = \frac{\sqrt{\pi}}{2} \sqrt{\frac{1}{N} \sum_{i=1}^{N} Z_i^2} \qquad (B-1)$$

where z_i are i.i.d. Rayleigh random variables having parameter $\sigma = \pi M\sqrt{2}$ is given by:

$$f_x(X) = \frac{2(\frac{N}{M^2})^N X^{2N-1}}{(N-1)!} \exp[-\frac{N}{M^2}X^2] \qquad (B-2)$$

Therefore:

$$\begin{aligned} \mathrm{E}[\hat{m}] &= \mathrm{E}[x] = \int_0^\infty X f_x(X) dX = \pi(N)M && \text{(B-3)} \\ \mathrm{var}[\hat{m}] &= \mathrm{E}[\hat{m}^2] - \mathrm{E}^2[\hat{m}] = (1-\pi^2(N))M^2 && \text{(B-4)} \\ \mathrm{E}[(\hat{m}-M)^2] &= \mathrm{E}[\hat{m}^2] - 2M\mathrm{E}[\hat{m}] + M^2 \\ &= 2\,(1-\pi(N))M^2 && \text{(B-5)} \end{aligned}$$

□

Proof of Lemma 4

The mean-squared value of the i-th order statistic of a set of N observations is given by [23]:

$$\mathrm{E}[n_{(i)}^2] = \frac{N!}{(i-1)!\,(N-i)!} \int_0^\infty x^2 F^{i-1}(x)\,[1-F(x)]^{N-i} f(x)\,dx \qquad (B-6)$$

where $F(x)$ is the Rayleigh cumulative density function (cdf). By making the substitution $\xi = \exp(-\frac{x^2}{2\sigma^2})$, Eq. (43) results. The expected value of the product of the i-th and j-th order statistics, where $i < j$, is given by [23]:

$$\mathrm{E}[n_{(i)}n_{(j)}] = \int_0^\infty dx \int_x^\infty dy\, xy\, f_{ij}(x,y) \qquad (B-7)$$

where

$$\begin{aligned} f_{ij}(x,y) &= \frac{N!}{(i-1)!\,(j-i-1)!\,(N-j)!} F^{i-1}(x)\,[F(y)-F(x)]^{j-i-1} \\ &\times\ [1-F(y)]^{N-j} f(x)\,f(y) \quad 1 \le i < j \le N \qquad \text{(B-8)} \end{aligned}$$

By making the following change of variables $\alpha = \exp(-\frac{x^2}{2\sigma^2})$ and $\beta = \exp(-\frac{y^2}{2\sigma^2})$, Eq. (44) results. □

ACKNOWLEDGMENTS

The authors are grateful to Dr. T. Loupas for his many helpful comments. They would also like to thank Prof. J.M. Thijssen and Prof. J.C. Bamber for providing the clinical and phantom images to them. Constantine Kotropoulos was supported by a scholarship from the State Scholarship Foundation of Greece and the Bodosaki Foundation.

REFERENCES

[1] Goodman, J.W., Statistical Properties of Laser Speckle Pattern, in *Laser Speckle and Related Phenomena*, J.C. Dainty, ed., pp. 9–75, (Springer-Verlag, Berlin, 1975).

[2] Abbott, J.G., and Thurstone, F.L., Acoustic speckle: theory and experimental analysis, *Ultrasonic Imaging 1*, 303–324 (1979).

[3] Smith, S.W., Wagner, R.F., Sandrik, J.M., and Lopez, H., Low contrast detectability and contrast/detail analysis in medical ultrasound, *IEEE Trans. Son. Ultrason. SU-30*, 156–163 (1983).

[4] Wagner, R.F., Insana, M.F., and Brown, D.G., Unified approach to the detection and classification of speckle texture in diagnostic ultrasound, *Optical Engineering 25*, 738–742 (1985).

[5] Insana, M.F., Wagner, R.F., Garra, B.S., and Shawker, T.H., Analysis of ultrasound texture via generalized Rician statistics, *Optical Engineering 6*, 743–748 (1985).

[6] Wagner, R.F., Fundamentals and Applications of Signal Detection Theory in Medical Imaging, in *Proc. SPIE*, Vol. 626, pp.761–765 (1986).

[7] Thijssen, J.M., Oosterveld, B.J., and Wagner, R.F., Gray level transforms and lesion detectability in echographic images, *Ultrasonic Imaging 10*, 171–195 (1988).

[8] Thijssen, J.M., Focal Lesions in Medical Images: A Detection Problem, in *Proceedings NATO-ASI on Mathematics and Computer Science in Medical Imaging*, M.A. Viergever and A. Todd-Prakopek, eds., pp. 415-440 (Springer, Berlin, 1988).

[9] Raeth, U., Schlaps, D., Limberg, B., Zuna, I., Lorenz, A., Van Kaick, G., Lorenz, W.J., and Kommerell, B., Diagnostic accuracy of computerized B-scan texture analysis and conventional ultrasonography in diffuse parenchymal and malignant liver disease, *J. Clinical Ultrasound 13*, 87–99 (1985).

[10] Insana, M.F., Wagner, R.F., Garra, B.S, Momenan, R., and Shawker, T.H., Pattern recognition methods for optimizing multivariate tissue signatures in diagnostic ultrasound, *Ultrasonic Imaging 8*, 165–180 (1986).

[11] Bamber, J.C., and Daft, C., Adaptive filtering for reduction of speckle in ultrasonic pulse-echo images, *Ultrasonics 24*, 41–44 (1986).

[12] Loupas, T., McDicken, W.N., and Allan, P.L., An adaptive weighted median filter for speckle suppression in medical ultrasonic images, *IEEE Trans. on Circuits and Systems CAS-36*, 129–135 (1989).

[13] Koo, J.I., and Park, S.B., Speckle reduction with edge preservation in medical ultrasonic images using a homogeneous region growing mean filter, *Ultrasonic Imaging 13*, 211–237 (1991).

[14] Lopes, A., Touzi, R., and Nezry, E., Adaptive speckle filters and scene heterogeneity, *IEEE Trans. on Geoscience and Remote Sensing GE-28*, 992–1000 (1990).

[15] Pitas, I., and Venetsanopoulos, A.N., *Nonlinear Digital Filters: Principles and Applications* (Kluwer Academic Publishers, Hingham MA, 1990).

[16] Loupas, T., and McDicken, W.N., Digital Image Formats: A Survey of Ultrasound Imaging Equipment, *Final Report for Project A-8323 of the Advanced Informatics in Medicine Programme of the EEC*, Department of Medical Physics and Medical Engineering, University of Edinburgh, U.K. (February 1990).

[17] Oosterveld, B.J., Thijssen, J.M., and Verhoef, W.A., Texture of B-mode echograms: 3-D simulations and experiments of the effects of diffraction, *Ultrasonic Imaging 7*, 142–160 (1985).

[18] Loupas, T., Digital Image Processing for Noise Reduction in Medical Ultrasonics, *Ph.D dissertation*, University of Edinburgh, U.K. (July 1988).

[19] Pitas, I., and Venetsanopoulos, A.N., Edge detectors based on nonlinear filters, *IEEE Trans. on Pattern Anal. and Machine Intelligence PAMI-8*, 538–550 (1986).

[20] Bovik, A.C., Huang, T.S., and Munson, D.C., A generalization of median filtering using linear combinations of order statistics, *IEEE Transactions on Acoustics, Speech and Signal Processing, ASSP-31*, 1342–1349 (1983).

[21] Papoulis, A., *Probability, Random Variables and Stochastic Processes* (McGraw-Hill, New York, 1984).

[22] Van Trees, H.L., *Detection, Estimation and Modulation Theory* (J. Wiley & Sons, New York, 1968).

[23] David, H.A., *Order Statistics* (J. Wiley & Sons, New York, 1980).

[24] Verhoeven, J.T.M, Thijssen, J.M., and Theeuwes, A.G.M., Lesion detection by echographic image processing: signal-to-noise ratio imaging, *Ultrasonic Imaging 13*, 238–251 (1991).

[25] Magnisalis, X., Kotropoulos, C., Pitas, I., and Strintzis, M.G., Use of Fractal Dimension in Signal Adaptive Filters for Speckle Reduction in Ultrasound B-mode Images, in *Proceedings of the Tenth Int. Congress on Medical Informatics MIE 91*, pp. 550–554 (Vienna, Austria, August 1991).